AGU PUBLICATIONS

JGR

Journal of Geophysical Research: Space Physics

RESEARCH ARTICLE
10.1002/2016JA022418

Key Points:
- Absence of westward electrojet and delay between the substorm onset and onset of DCNA
- Presence of pronounced Pc5 oscillations at Maitri during DCNA event
- Estimated energy bands are in agreement with the observation from GOES

Correspondence to:
J. K. Behera,
jayanta.sssj@gmail.com

Citation:
Behera, J. K., A. K. Sinha, G. Vichare, O. Kozyreva, R. Rawat, and A. Dhar (2016), Dayside cosmic noise absorption at the equatorward boundary of auroral oval as observed from Maitri, Antarctica ($L = 5$; CGM 62.45°S, 55.45°E), *J. Geophys. Res. Space Physics*, *121*, doi:10.1002/2016JA022418.

Received 21 JAN 2016
Accepted 4 APR 2016
Accepted article online 7 APR 2016

Dayside cosmic noise absorption at the equatorward boundary of auroral oval as observed from Maitri, Antarctica ($L = 5$; CGM 62.45°S, 55.45°E)

Jayanta K. Behera[1], Ashwini K. Sinha[1], Geeta Vichare[1], Olga Kozyreva[2], Rahul Rawat[1], and Ajay Dhar[1]

[1]Indian Institute of Geomagnetism, New Panvel (W), Navi Mumbai, India, [2]Institute of Physics of the Earth, Moscow, Russia

Abstract On 02 April 2011, a couple of cosmic noise absorption (CNA) events were detected at Maitri, Antarctica ($L = 5$; CGM 63.14°S, 53.69°E) confining to nighttime and daytime. One of the two events that occurred during night hours was caused due to auroral substorm onset. The current study focuses on the later CNA event, which was recorded during daytime (10:00–13:00 magnetic local time (MLT), MLT = UT-1, at Maitri, Antarctica). We refer to this CNA event as dayside CNA (DCNA) event. Absence of westward electrojet during DCNA confirms its dissimilarity from auroral substorm absorption events. A comparison has been made between the DCNA event of 02 April 2011 with that of 14 July 2011, a day with substorm activity when Maitri is in dayside but without DCNA event. The comparison has been made in the light of interplanetary conditions, imaging riometer data, ground magnetic signatures, GOES electron flux density, and associated pulsations. The study shows that stronger prolonged eastward interplanetary electric field favors the occurrence of DCNA event. It is concluded that DCNA event is due to the gradient curvature drift of trapped nonrelativistic electrons in the equatorial plane. Estimated energy of trapped electrons using azimuthal drift time for a set of ground stations within the auroral oval confirms the enhancement in electron fluxes in the same energy band as recorded by geostationary satellites GOES 13 and GOES 15. The reason for precipitation of electrons is expected to be the loss cone scattering caused by wave-particle interaction triggered by ULF waves.

1. Introduction

For many decades, cosmic noise absorption phenomenon is possibly considered as the most reachable and handy proxy to decipher the energetic particle precipitation at high-latitude ionosphere, mostly in *D* region [*Little and Leinbach*, 1959]. The process of deposition is either in the open field line region at the dayside of magnetosphere or in the closed field line region in the nightside [*Newell and Meng*, 1992]. The nightside precipitations is mainly due to high energetic electrons in the energy range of >20 keV inside the auroral region [e.g., *Hargreaves*, 2007]. Softer electrons (<10 keV) are responsible for auroral display and in some part for intensification of auroral electrojet in ionospheric *E* and *F* regions. *Semeter et al*. [2001] have used new multispectral imager and associated multispectral analysis to understand the connection between the auroral morphology and the auroral optical spectrum in the same region of ionosphere. However, harder electrons such as 30 keV to few MeV can penetrate deeper in to the ionosphere and subsequently affect the composition of the middle atmosphere [*Codrescu et al*., 1997]. The use of wide beam riometer for the particle precipitation could not provide the spatial information of the cosmic noise absorption (CNA) pattern and later was replaced by advanced arrays of riometers forming different beams in 1990 and are called imaging riometer [*Detrick and Rosenburg*, 1990]. The basic technique of imaging riometer is to receive the radio noises from the interstellar region at a particular radio frequency [*Honary et al*., 2011]. Indian Institute of Geomagnetism operates an imaging riometer of 4×4 antenna system at Maitri, whose operating frequency is 38.2 MHz. CNA is often measured in decibel and it can be calculated by simply following equation

$$A = \log_{10}(S_1/S_2) \tag{1}$$

$$A = 4.6\times10^{-5}\int \frac{N_e \nu . dl}{\nu^2 + (\omega \pm \omega_H \cos\theta)^2} \tag{2}$$

where S_1 and S_2 are the cosmic radio noise signal received at 38.2 MHz during disturbed and quiet ionospheric conditions, respectively. Equation (2) states the Appleton-Hartree equation [*Nyland*, 2007], where N_e and ν are, respectively, the local electron density and collision frequency and $\omega_H \cos\theta$ is the longitudinal component of the electron gyrofrequency. The plus and minus signs indicate the two different types of

polarization of the incoming wave. ω is the angular frequency of the wave propagating at an angle θ with the geomagnetic field along the path *l* of which *dl* is the small element.

Various types of CNA are attributed to different solar-terrestrial phenomena such as storm sudden commencement-related CNA, X-ray flare-generated CNA, and substorm-related CNA [*Stauning*, 1996]. Substorm-related CNAs during midnight hours are very frequent and well studied [*Ranta et al*., 1999; *Lopez and Lui*, 1990; *Liang et al*., 2007]. However, these CNAs can sometimes be observed in the extended range of local time depending upon the latitudinal and longitudinal expansion of auroral oval, which is a consequence of the ionospheric plasma convection due to injection of energetic particles from the tail during midnight sector [*Ansari*, 1964]. Many researchers have discussed about the morningside CNA as well as prenoon hour CNAs. However, very few cases of dayside CNA event from subauroral locations and no dayside CNA (DCNA) event from Maitri have been reported so far. Additionally, very little is known about its possible cause. Researchers have suggested that the higher-energy electrons (>20 keV) are responsible for high-latitude dayside cosmic noise absorption [*Matthews et al*., 1988; *Newell and Meng*, 1992; *Østgaard et al*., 1999]. It is shown that the electrons associated with central plasma sheet, being injected in the nightside of the magnetotail, mostly in midnight hours and further fall into loss cone during gradient-curvature drift in the inner magnetosphere. This kind of precipitation at high latitude is possible due to cyclotron resonance between the electrons in the Earth's radiation belt and chorus waves causing pitch angle scattering into the loss cone during different geomagnetic activities [*Ding et al*., 2013; *Su et al*., 2014; *Xiao et al*., 2009, 2010, 2014]. Presence of Pc5 pulsation and whistler mode VLF emission during the morningside precipitation and further production of CNA are well-known phenomena at high latitude (L = 5.1–5.5) [*Manninen et al*., 2010]. This whistler mode chorus is observed in the frequency range ~0.5–2.5 kHz outside the plasmapause and is one of the drivers of energetic electron precipitation especially in the dawn sector [e.g., *Pasmanik and Trakhtengerts*, 1999; *Bortnik and Thorne*, 2007; *Gołkowski and Inan*, 2008].

CNA may also differ in many aspects such as time of occurrences, magnetic signatures, and intensity. For example, the auroral substorms are often associated with the westward electrojet and they are almost concurrent. Generally, substorms occur in the premidnight sector [*Frey and Mende*, 2006] and populate the inner magnetosphere due to field-aligned propagation of energetic particles immediately after the reconnection process starts [*Spanswick et al*., 2007; *Liang et al*., 2007]. Hence, the westward electrojet intensification and CNA onset are almost instantaneous with respect to auroral substorms and have been observed at Maitri, Antarctica [*Behera et al*., 2014]. Hence, there must be a significant westward signature if a CNA enhancement is observed in any location inside the auroral oval. However, in the current study, the CNA event that falls in the dayside has no simultaneous signatures of westward electrojet at the same site of observation in Maitri.

Interplanetary parameters are key to understand the cosmic noise absorption pattern, notably the effect of interplanetary magnetic field (IMF), solar wind pressure, and interplanetary electric field [*Sandholt and Newell*, 1996; *Kavanagh et al*., 2004; *Behera et al*., 2014]. Changes in dynamic pressure due to solar wind velocity could lead to the enhancement in precipitation. It is statistically shown that the average CNA becomes larger with increasing level of solar wind velocity [*Kavanagh et al*., 2004]. Basically, solar wind velocity has to be the driving cause for the geomagnetic activities and a proxy to total energy input to the magnetosphere. Characteristics of southward component of interplanetary magnetic field (IMF B_z) is crucial for understanding different types of CNA observed at high latitude. For example, northward turning of IMF B_z after being southward for a certain duration of time would give rise to onset of substorms at high latitude. The duration and the extent of IMF B_z decide the level of substorm activity. Moreover, during high-speed solar wind events, it is shown that a negative IMF B_z has produced higher CNA across all L shells and magnetic local time (MLT), up to 100% higher than positive IMF B_z [*Kavanagh et al*., 2012]. However, northward IMF can also produce CNA but at the poleward edge of the cusp with auroral signatures [*Sandholt et al*., 1996; *Øieroset et al*., 1997; *Sandholt et al*., 2000]. Nevertheless, the longer sustainability of larger interplanetary electric fields is more appropriate to correlate with the level of CNA production at high latitude due to substorm activity [*Behera et al*., 2015].

In the current study, initially, we have defined the characteristics of a dayside CNA event, and thereafter, a comparison is made between two different days of 02 April 2011 and 14 July 2011. Although the substorm occurrences took place on both these days, the dayside CNA occurred only on one of the days. The study location is Maitri, Antarctica (L = 5; geographic 70.75°S, 11.75°E; corrected geomagnetic (CGM) 62.45°S, 55.45°E). The above

exercise was done to identify the necessary and sufficient condition for the occurrence of the dayside CNA event. The comparative study has been carried out in the light of ground magnetic signatures, riometer signatures, interplanetary conditions, GOES satellite observation of particle fluxes in different energy bands (40, 75, 150, 275, and 475 keV), and associated pulsations. Additionally, successive delays of the onset of CNA at longitudinally distributed stations inside the auroral oval have also been examined. Temporal delay between the onset of the substorm and onset of CNA at Maitri has been attributed to the azimuthally gradient drift of energetic electrons. We use this delay time in the gradient-curvature drift equation [*Beharrell et al*., 2015] to get an order of energy estimate of the electron fluxes. The abrupt enhancements in electron fluxes in certain energy bands as observed from different GOES satellites could result into the occurrences of dayside CNA event as observed on 02 April 2011.

2. Data Sets

The data recorded by imaging riometer installed at Indian Antarctic station (Maitri) have been used for the cosmic noise absorption study. A 4×4 array of imaging riometer with operating frequency of 38.2 MHz has been installed at this location and is in operation since austral summer of 2010 at Maitri, Antarctica. The antenna consists of 16-element dipole-phased array which provides 16 imaging beams and a single wide beam over a 200×200 km field of view. The horizontal beam width is approximately 20 km at an approximate height of 90 km (*D* region) near the zenith, and all the beam data were sampled at 1 s. Moreover, this riometer has both wide beam and narrow beam (image beam) facility; the wide beam provides the enhanced CNA information quantitatively, whereas image beam provides the spatial evolution of the CNA patterns. Additionally, Indian Institute of Geomagnetism also runs a digital fluxgate magnetometer (DFM) at Maitri since 2003. The sampling rate of data acquisition of the DFM is 1 s with 1 nT resolution. The imaging riometer and DFM are operated together at Maitri to study the substorm-related particle precipitation characteristics and the dynamics of auroral electrojet current systems. Bharati (CGM 74.4°S, 97.2°E) is another newly commissioned Indian Antarctic station, where characteristics of poleward substorm studies are going on [*Singh et al*., 2012].

To identify the substorm onset time and its strength, we have used *AL* index and *Wp* index from the WDC, Kyoto site. Recently, *Wp* (wave and planetary) index has been introduced by *Nose et al*. [2012] as a new and more authentic indicator of substorm onsets [*Thomas et al*., 2015]. This index shows the wave power of the Pi2 pulsation at low latitude, which was derived from geomagnetic data from 11 low-latitude stations. *Singh et al*. [2012] has shown the importance of fixing criteria on *AE*/*AL* index enhancement/depression to identify a substorm. For identifying substorm onset, we impose the condition on *AL* that there should a transient depression of more than 150 nT within a time span of 2 min. *SYM-H* and *Dst* index data have been used as a proxy for the ring current enhancement during the course of the observed events. For interplanetary parameters such as interplanetary magnetic fields, solar wind velocity, and interplanetary electric field, data have been taken from the OMNIWEB data center (http://omniweb.gsfc.nasa.gov/form/omni_min.html). The in situ measurements of energetic electron flux injections have been obtained from GOES 13 satellite.

The GOES consists of energetic particle sensor and magnetometers as part of environment monitoring instruments. These energetic particle fluxes are given as 1 min/5 min average values, and the vector magnetic field data are given by 1 min average values. Flux values for integral electron channels ($E > 0.8$ MeV, $E > 2.0$ MeV) and electron flux 40–475 keV data can be collected from the CDAWEB website of NASA (http://cdaweb.gsfc.nasa.gov/cgi-bin/eval1.cgi). In the current study, we have used GOES 13 and GOES 15 energetic particle sensor Magnetospheric Electron Detector 1 min electron flux data in the energy band of 40–475 keV. These data are mainly provided by NOAA National Geophysical Data Center and Space Weather Prediction Center (sem.goes@noaa.gov).

In order to study the global Pc5 oscillation characteristics, magnetic field variations as recorded by DFM were used from some of the INTERMAGNET stations. Geomagnetic component variation data with 1 min resolutions were taken in the International Association of Geomagnetism and Aeronomy 2002 format from the INTERMAGNET data website (http://www.intermagnet.org/data-donnee/data-eng.php). The stations were taken arbitrarily to see the global Pc5 oscillations during the event days. Geographic and geomagnetic coordinates of the INTERMAGNET stations are given in Table 1. For the current study, riometer data were used from some of the stations such as DAWS, HSIM, GILL, RABB of NORthern Solar Terrestrial ARray (NORSTAR)

Table 1. Geographic and Geomagnetic Coordinates of the INTERMAGNET Stations, Taken for Global Pc5 Observation

Serial No.	Stations	Geographic Latitude (°S)	Geographic Longitude (°E)	Geomagnetic Latitude (°S)	Geomagnetic Longitude (°E)
1	CSY	−66	110	75	184
2	CNB	−35	149	41	227
3	ASP	−23	133	31	208
4	PPT	−17	210	14	285
5	ASC	−7	345	1	304

riometer chain (http://aurora.phys.ucalgary.ca/norstar/index.html), and MCQ station of Australian riometer chain. Coordinates for these stations are provided in Table 2.

3. Observations

3.1. A Dayside Absorption Event With Interplanetary Conditions

On 02 April 2011, enhancement in the CNA occurred twice at Maitri at ~06:40 UT and ~11:44 UT. To identify CNA onset, we impose the condition that there should be an enhancement of more than 0.3 dB within 2 min. This criterion is an extension of the criterion (CNA >0.2) given in *Behera et al*. [2015] to identify a CNA event at Maitri. The time constraint was added in order to identify the CNA event at different stations to examine CNA characteristics at longitudinally distributed stations inside the auroral oval during the substorm on 02 April 2011 (mentioned in section 5; Figure 9). Just by looking at the transient enhancement, it was difficult and ambiguous. Occurrence durations of these two events were approximately 1 h, 12 min and 1 h, 54 min, respectively. Associated geomagnetic activities were completely different for these CNA events. In Figure 1 , the top two plots depict *AL* index and *Wp* index which are essentially indicator of the substorm onset. The next plot represents the horizontal component of geomagnetic field at Maitri. The fourth plot from the top represents wide beam CNA data. The calculation of CNA was done using equation (1). The quiet day curve for cosmic noise signal have been computed by following strict criteria [*Behera et al*., 2014]. The second last plot represents *SYM-H*, and the bottom most plot shows the keogram of the imaging riometer which gives the image plot of cosmic noise enhancement across the field of view of imaging riometer at Maitri.

Close observation of *AL* index reveals onset of two substorms that have occurred at 06:40 UT and 11:20 UT. For both events the *AL* index has gone down to ~ −700 nT and ~ −750 nT, respectively. Interestingly, we have observed CNA enhancement in the riometer data related to these substorm occurrences. However, the onset time for both the CNA did not coincide with the substorm occurrences. The first event for which substorm and CNA onset coincide is well understood and can be termed as auroral substorm absorption events where charged particles precipitated in the auroral oval during substorm process [*Behera et al*., 2015]. Additionally, during auroral substorm absorption events, occurrence of westward electrojet is commonly observed at the site of the observation. The later CNA event also seems to be related to substorm activity. However, a clear delay of 24 min between the onset of substorm and onset of CNA is observed. There is no indication of the intensification of westward electrojet in the *H* component variation. The fourth panel represents the image plot of the intensification of the CNA and its areal coverage. It can be clearly observed that both the CNA

Table 2. Geographic and Geomagnetic Coordinates and *L* values of NORSTAR and Space Weather Service (SWS) Australian Stations, Taken for Riometer Observations

Serial No.	Stations	Geographic Latitude (°S)	Geographic Longitude (°E)	CGM Latitude (°S)	CGM Longitude (°E)	*L* values (in *Re*)
1	MCQ	−54.16	158.00	−64.21	247.09	5.3
2	DAWS	64.05	220.89	65.95	274.68	6.1
3	FSIM	61.76	238.77	67.21	295.10	6.7
4	RABB	58.22	256.32	66.75	319.84	6.5
5	GILL	56.38	265.38	65.90	333.74	6.09
6	MAI	−70.75	11.75	63.14	53.69	5

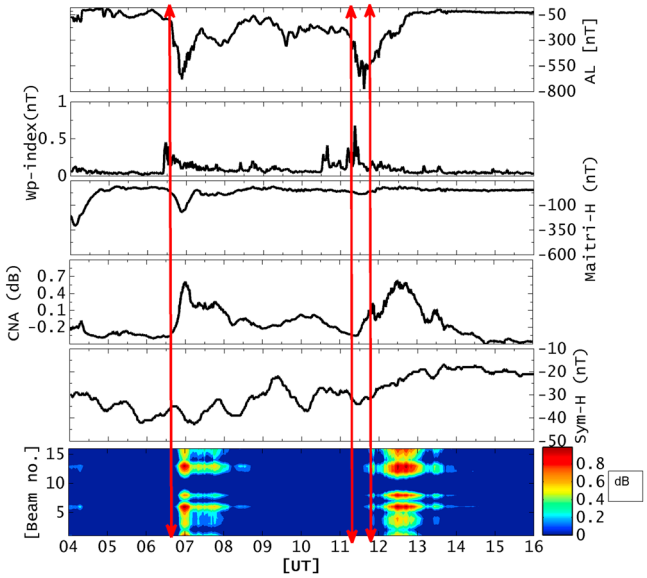

Figure 1. Ground signatures of CNA events on 02 April 2011 at Maitri. (first panel) *AL* index and (second panel) *Wp* index, respectively. (third and fourth panels) The variation in the horizontal component of geomagnetic field and wide beam CNA at Maitri, respectively. (fifth panel) *SYM-H* and (sixth panel) the keogram of the imaging riometer. The extreme left solid line indicates the onset of auroral substorm absorption events, whereas the middle solid line represents the onset of the second substorm, and extreme right solid line shows the onset of CNA at Maitri. The delay between the onset of substorm and CNA onset at Maitri is a typical characteristics of DCNA.

enhancements are very localized, but the intensity of the later event is high compared to earlier event. The delay (in onset) for the second event is clearly visible in this image also. Interestingly, *SYM-H* (<-30 nT) indicates the presence of a moderate geomagnetic storm and enhancement of ring current during 02 April 2011.

In Figure 2, solar wind velocity (V_{sw}), solar wind pressure (P_{sw}), interplanetary parameters such as IMF B_z and IMF B_y, and interplanetary electric field components (IEF E_y and IEF E_z) have been plotted, respectively, from top to bottom plots. It is observed that IMF was southward for a while before the onset of the substorm in the events. However, IMF B_z remained southward for a longer time ~2 h before the onset of the second event as compared to the first one. Solar wind velocity was initially moderate ~400 km/s and picked up to 600 km/s later. The solar wind pressure indicates no drastic change during the course of the events. It was steady with a value between 1.5 and 2 nPa. Interplanetary electric field (IEF $= -V_{sw} \times B_z$) depends quantitatively upon solar wind velocity and IMF B_z, and its direction depends upon the IMF B_z orientation. The direction of IEF E_y is eastward or westward, depends upon whether IMF B_z is southward or northward, respectively. IMF B_y was consistently westward during both the substorms with eastward turning on couple of occasions such as ~08:40 and ~11:10 UT. Corresponding to B_y orientation IEF E_z was northward with couple of southward turnings. Average strength of IEF E_z was <2.5 mV/m during both the substorms. In this work, we are concentrating on DCNA event, i.e., the event that occurred in the later time (11:00–14:00 UT) during 02 April 2011. Prior to the event, IEF was eastward for more than 1 h and turned westward before the onset of the substorm. The value of IEF was approximately 5 mV/m, which is larger than that during the auroral substorm CNA event.

Generally, a substorm is accompanied by westward electrojet which is observed as a significant depression in the *H* component variation in the geomagnetic field inside the auroral oval. At Maitri, signatures of westward electrojet have been reported during substorm onsets [*Behera et al*., 2015]. However, the onset of westward electrojet, sometimes, matches with the onset of substorm or may get delayed depending upon the location of study. On 02 April 2011, although two CNA events were observed, westward electrojet is observed only for the first event, whereas we do not observe any westward electrojet for the second event of CNA during the later substorm occurrence despite the fact that the later substorm was relatively intense. Also, for the second event clear delay between the substorm onset and CNA onset is quite evident. The detail discussion on the delay has been presented in section 5.

3.2. A Dayside No-Absorption Event With Similar Interplanetary Conditions

In contrast to the event of 02 April 2011, a substorm that occurred on July 14 2011 during 10:00–11:30 UT is presented here. Figure 3, similar to Figure 1, represents the two topmost plots showing *AL* index and *Wp* index. Next two plots represent the variation in *H* component and wide beam CNA at Maitri, respectively. The second last plot depicts *SYM-H* and the bottom most plot shows the keogram of imaging riometer.

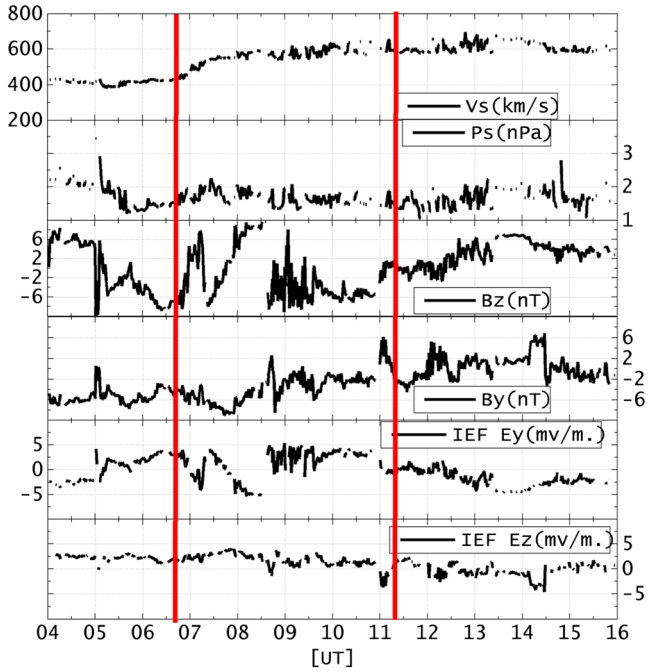

Figure 2. Interplanetary conditions during 02 April 2011. The two topmost plots show the IMF B_z and solar wind velocity V_{sw}. The next two bottom plots represent the solar wind pressure P_{sw} and IEF E_y. The solid lines indicate the time of onset of the substorms.

The substorm has occurred at ~10:10 UT on 14 July 2011. *AL* index showed a strong depression of ~800 nT. *Wp* index, during this time, was pronounced and certainly confirmed the occurrence of substorm. However, during this substorm, Maitri did not show any production of CNA or westward electrojet. Moreover, *SYM-H* indicates absence of any ring current enhancement.

Figure 4 represents the interplanetary parameters during the event of 14 July 2011. Although IMF B_z was southward before and after the onset of the substorm, the level of IMF B_z was less (~ −2nT) compared to the event of 02 April 2011. It was only ~ −2 nT. Solar wind velocity was quite steady (~500 km/s). Although it is above the average solar wind velocity, no abrupt change or enhancement was observed during the substorm. Same was the case for solar wind pressure. IMF B_y was initially eastward then turned westward during the onset of the substorm. We notice that the interplanetary electric fields (IEF E_y and IEF E_z) parameters are consistently low (0–1 mV/m) during the substorm.

3.3. GOES 13 Observation During Both the Events

Despite the fact that both days had fair substorm activity, enhancement in the CNA during daytime occurred only on 02 April 2011. In order to identify the possible cause of the differences observed for the studied days, we examined the particle data from GOES 13 and GOES 15. Figure 5 represents the fluxes of electrons of different energy levels for the days of 02 April 2011 and 14 July 2011. Both the plots represent the fluxes of nonrelativistic electrons within the range of 40–475 keV. The left plot corresponds to the event of 02 April 2011 and the right plot corresponds to 14 July 2011. The two black solid lines represent the time of onset of the substorms at ~11:20 UT for 02 April 2011 and ~10:10 UT for 14 July 2011. During the substorm occurrence at ~11:20 UT on 02 April 2011, Maitri was at ~10:20 MLT, GOES 13 was at 06:00 MLT, and GOES 15 was at 05:00 MLT. For the substorm event of 14 July 2011 which occurred at ~10:10 UT, Maitri was at ~09:10 MLT, GOES 13 was at 05:00 MLT, and GOES 15 was at 04:00 MLT. Sudden enhancement is observed in all the electron fluxes during both the events. However, it can be seen that fluxes in the energy ranges of 150 keV and 275 keV have larger enhancements at the substorm onset

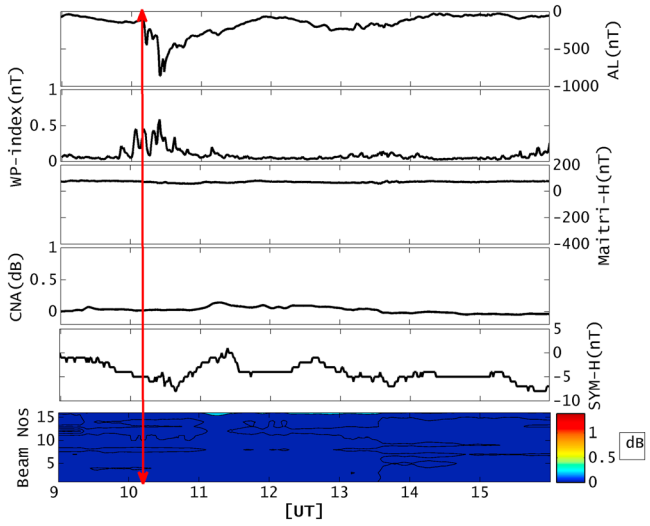

Figure 3. Same as Figure 1 but for 14 July 2011 substorm event.

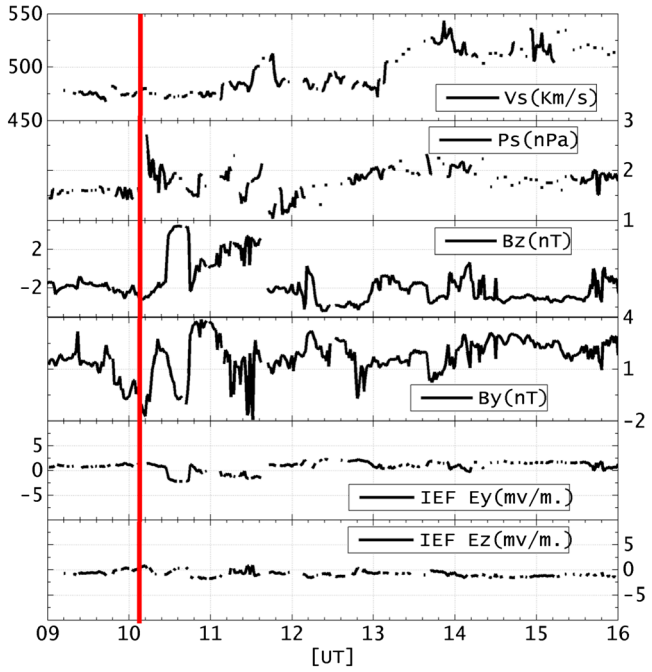

Figure 4. Same as Figure 2 but on 14 July 2011.

time on 02 April 2011 compared to other day, i.e., 14 July 2011.

Fluxes in the energy ranges of 45 and 75 show approximately same order of enhancement during both the days. At the onset, the magnitudes of the 150 keV and 275 keV fluxes were 4×10^3 ($cm^{-2}\,s^{-1}\,sr^{-1}\,keV^{-1}$) and 6×10^2 ($cm^{-2}\,s^{-1}\,sr^{-1}\,keV^{-1}$), respectively, which later increased up to 7×10^4 ($cm^{-2}\,s^{-1}\,sr^{-1}\,keV^{-1}$) and 5×10^3 ($cm^{-2}\,s^{-1}\,sr^{-1}\,keV^{-1}$), respectively. Whereas, in case of 14 July 2011, magnitudes of similar energetic electrons were7×10^3 ($cm^{-2}\,s^{-1}\,sr^{-1}\,keV^{-1}$) and 1×10^3 ($cm^{-2}\,s^{-1}\,sr^{-1}\,keV^{-1}$), respectively, which later increased up to 3×10^4 ($cm^{-2}\,s^{-1}\,sr^{-1}\,keV^{-1}$) and 3×10^3 ($cm^{-2}\,s^{-1}\,sr^{-1}\,keV^{-1}$), respectively. Hence, more precisely, we can find 16.5 times increment in the flux density of 150 keV and 7.3 times in 275 keV electrons during 02 April 2011, whereas only 3 times increment in density of 150 keV and 2 times in 275 keV electrons during 14 July 2011. Flux enhancement in the energy range of 475 shows increment of only 100 ($cm^{-2}\,s^{-1}\,sr^{-1}\,keV^{-1}$) during the onset of 02 April 2011 compared to 14 July 2011, which is less significant in comparison while discussing the cases of 150 and 275 keV energy bands.

3.3.1. Evolution of Electron Cloud Observed by GOES 13 and 15 for DCNA

Here we are examining the evolution of electron fluxes for 02 April 2011, on which we observed DCNA event. Electron flux data during the substorm onset on 02 April 2011 were available for two GOES satellites (GOES 13 and GOES 15) separated in MLT by 1 h during the substorm onset. At the substorm onset, GOES 13 was located at ~06:00 MLT and GOES 15 was located at ~05:00 MLT. Hence, GOES 15 was closer to magnetic midnight than GOES 13 and was likely to encounter with the electron clouds earlier than GOES 13. Figure 6 shows the electron fluxes of 40–475 keV range during the substorm period. Substorm onsets at ~11:20 UT, and we can clearly see the electron clouds encountered by both the GOES satellites. However, GOES 15 shows enhancements in the electron flux for all the energy ranges prior to these observed in GOES 13. A delay of 3–7 min in peak enhancement of electron flux was observed between the two satellites. We have observed shorter delay times for higher-energy electron flux drift and longer time delay associated with lesser energetic flux. For example, maximum time delay of ~7 min is observed between the peak enhancement of electron flux in 40 keV energy band as detected by GOES 13 and GOES 15. Electron fluxes of energy 40 keV and 75 keV show gradual enhancement from the time of substorm onset and exhibit very slow recovery, thereby signifying moderate loss of electron fluxes in these energy bands. On the contrary, fluxes of energy 150 keV and 275 keV show delayed and sharp enhancements with steep recoveries, indicating the loss of electrons for these energy bands. Hence, electrons in these energy bands are more likely to precipitate resulting in to the observed CNA. Enhancement in 475 keV band is not so significant.

4. Global Pc5 (2–7 MHz) Waves Observed With DCNA

For decades, it has been proved theoretically as well as ground and satellite [*Sinha et al.*, 2005] observations that Pc5 pulsation has a great role in controlling the precipitation of charged particles at high latitude [*Kremser et al.*, 1981; *Kleimenova et al.*, 1997, 2005]. Together with VLF chorus, ULF pulsations are typically observed at auroral latitudes in the morning sectors and have close relation with loss of particles either due to parallel accelerated electrons in field line resonance process [*Nosé et al.*, 1998] or due to pitch angle

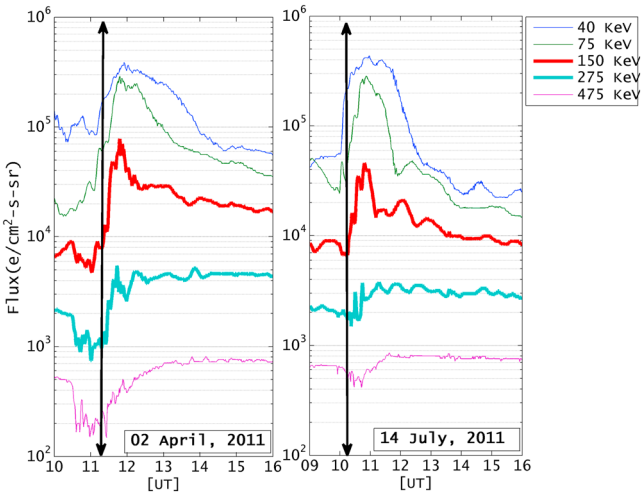

Figure 5. The 1 min resolution data of 40–475 keV electron flux densities by GOES 13 for 02 April 2011 and 14 July 2011. The solid bars of both the plots indicate the onset of substorm for these days; for example, 11:20 UT is the onset time of substorm on 02 April 2011 and 10:10 UT is the onset time of substorm on 14 July 2011.

scattering [*Spanswick et al.*, 2005]. Hence, in order to examine the presence of global Pc5 pulsation, we have taken magnetometer data from the selected stations from INTERMAGNET. The location of the selected stations is given in the Table 1. In Figure 7, the *H* component of the selected stations filtered at Pc5 pulsation range (2–7 MHz) for the duration of 10:00–14:00 UT on DCNA and no DCNA day have been plotted. The left figure is for 02 April 2011 and the right figure is for 14 July 2011. Note that the stations used here are from different MLT and latitudinal sectors. The presence of global Pc5 activity can be seen on both the days. Being in the auroral zone, the pulsation activity was strongest at CSY station on both days. Oval Variation, Assessment, Tracking, Intensity, and Online Nowcasting (OVATION) model provides the auroral zone boundary, position, and intensity of precipitation (http://sd-www.jhuapl.edu/Aurora/ovation/ovation_display.html). On 02 April 2011, OVATION plot for the auroral oval confirms that (plot is not shown here) CSY station was located well within the auroral oval, whereas rest of the stations mentioned in Table 1 were far away from the auroral oval. Unfortunately, there is no plot available for 14 July 2011 during the substorm period (10:00–12:00 UT).

Near the onset of the substorm (marked by vertical lines) large-amplitude pulsations are observed at almost all stations during both days. However, on 14 July, the amplitude of the pulsation activity reduced significantly after the recovery of the substorm (11:00 UT onward), while on 2 April, fairly good amplitude pulsations were observed for longer duration.

DFM at Maitri collects geomagnetic data at 1 s sampling interval. The collected data are then filtered in Pc5 range(1–7 MHz). Dynamic spectra for both the days have been constructed and are shown in Figure 8. The fast Fourier transform was carried out using sliding window of 1024 points (~17 min) with an extra overlap of 50% points. In Figure 8, the dynamic spectra of both days clearly show the presence of pulsation activity in the Pc5 range during the substorm activity for each days. However, Pc5 pulsation activity is seen more pronounced during the day when DCNA was present compared to the day of no DCNA (14 July 2011). Figures 8a and 8b represent the dynamic spectra of raw *H* component on 02 April 2011 and 14 July 2011, respectively. The time series of *H* were then filtered in the Pc5 range (2–7 MHz) and have been shown in Figures 8c and 8d for 02 April 2011 and 14 July 2011, respectively. A clear trail of Pc5 oscillations during the event of 02 April 2011 (which shows DCNA event) with peak

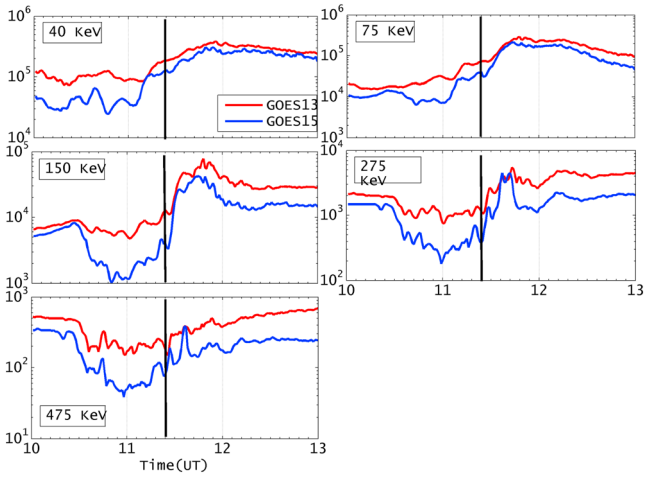

Figure 6. Electron cloud of energy bands 40–475 keV encountered by GOES 13 and GOES 15 during the substorm on 02 April 2011. At 11:20 UT (approximate onset time of substorm), GOES 13 was located at $X = -0.101$, $Y = -6.508$, and $Z = 1.173$ (R_E, GSM) and GOES 15 was at $X = -1.659$, $Y = -6.275$, and $Z = 1.6$ (R_E, GSM).

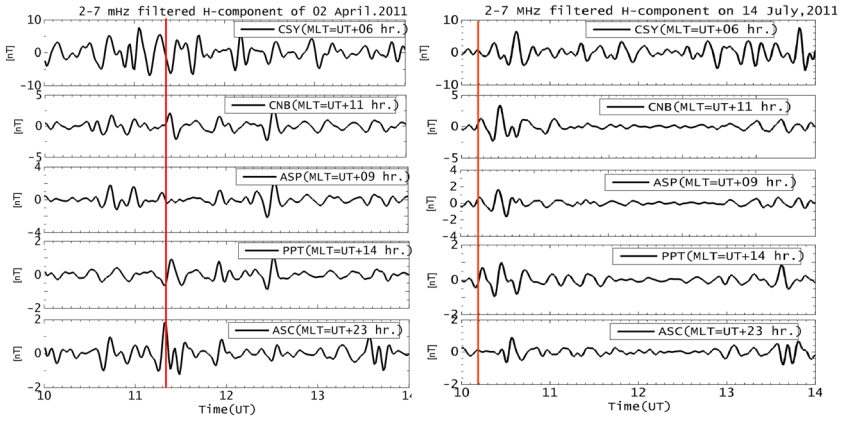

Figure 7. (left) The 2–7 MHz filtered *H* component at selected stations for the interval of 10:00–14:00 UT on 02 April 2011. (right) Same as the left plot but for 14 July 2011. The stations are arranged with decreasing order of latitudes. All stations are of different longitudes.

to peak amplitude of ~25 nT is seen, whereas the same for the event of 14 July 2011 (not showing DCNA) is only ~8 nT.

5. Discussion

For the first time, a comparative study has been made between the days of substorm occurrences with and without dayside CNA at Maitri, Antarctica, which can be useful to indentify the possible cause of dayside absorption events. DCNAs are not found to be associated with auroral westward electrojet, while nighttime CNAs are mainly accompanied with westward electrojets [*Behera et al.*, 2015]. Although both of events occurred during substorm activity, however, many a dissimilarities have been observed during these days in terms of interplanetary conditions, particle flux density, and amplitude of Pc5 pulsations.

While studying the interplanetary parameters such as solar wind velocity, IMF B_z, duskward interplanetary electric field, and solar wind pressure during the DCNA and no DCNA event days, it is clear that substorm occurred when IMF B_z was southward. However, we observe significant difference between the state and duration of southward IMF B_z during second substorm event of 02 April 2011 (11:00–13:00 UT) and the substorm event (10:00–12:00 UT) on 14 July 2011. On 02 April 2011, the southward IMF B_z decreased up to -6 nT (couple of times dipping below -6 nT), and it was consistently southward for ~2 h from ~09:00 UT onward. The solar wind was high (~600 km/s). Consequently, the interplanetary electric field was consistently eastward for couple of hours (5 mV/m). Whereas, on 14 July 2011, the maximum southward IMF B_z was <-2 nT, and it was southward for <1.5 h, although the solar wind velocity during this time was above

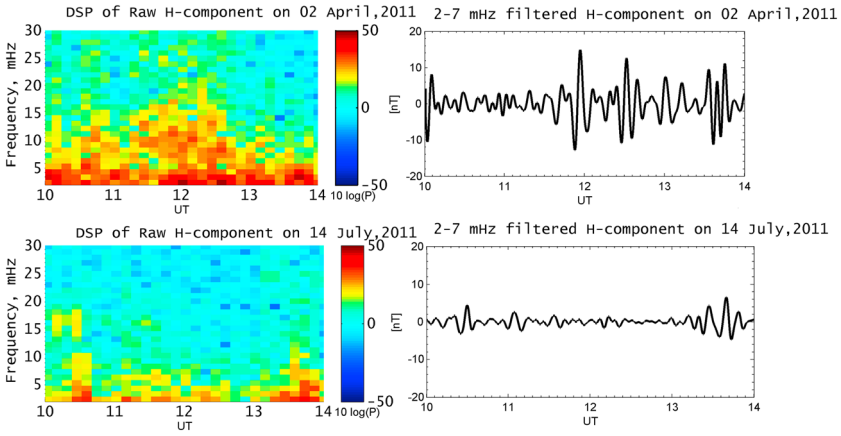

Figure 8. The dynamic spectra of raw *H* component at Maitri location on (a) 02 April 2011 and (b) 14 July 2011, respectively. The filtered *H* component in Pc5 pulsation range (~1–7 MHz) on (c) 02 April 2011 and (d) 14 July 2011, respectively.

average (<500 km/s). The interplanetary electric field, though eastward, was small (~1 mV/m). We believe that effects of IMF B_y and corresponding IEF E_z during the DCNA and no DCNA days will have very minor contribution to production of CNA. Basically, IMF B_y decides the longitudinal extent or the azimuthal range of substorm westward electrojet [*Arun et al*., 2005; *Friis-Christensen and Wilhjelm*, 1975]. Polarity of B_y governs the dawn-dusk shift of two-cell current system at high latitude. *Rodger et al*. [1984] showed the local time shift of Harang discontinuity depending upon the polarity of IMF B_y. However, this study precisely examines the characteristics of CNA during daytime at Maitri, where no signature of auroral electrojet is evident. The reason for DCNA is mainly the precipitation of large eastward drifted electron flux which is mostly controlled by IMF B_z and IEF E_y.

GOES 13 observation is helpful in understanding the difference between the electron flux density involved in these two events. If we compare the time windows of the two events, i.e., 11:00 UT onward for 02 April 2011 and 09:00 UT onward for 14 July 2011, wherein substorm have occurred, strong CNA is observed at Maitri on first day, while as the other day does not reflect any CNA at Maitri. Electron flux data shown in Figure 5 for subrelativistic energy range (40 keV, 75 keV, 150 keV, 275 keV, and 475 keV) show clear differences in the flux densities. For both the days, enhancements in the electron flux in these above energy ranges are seen at the substorm onset. However, electron fluxes during the DCNA day (02 April 2011) show increase by 16.5 times and 7.3 times in the energy bands of 150 and 275 keV, respectively, whereas respective increments during 14 July 2011 are 3 times and 2 times only (Figure 5). A close scrutiny of 02 April 2011 event based on the observations from two geostationary satellites GOES 13 and GOES 15 shows that both the satellites encountered the electron cloud at slightly different times. During the onset of substorm, GOES 13 and GOES 15 were located at 06:00 MLT and 05:00 MLT, respectively, which means that GOES 15 was closer to magnetic midnight than GOES 13.An early encounter by GOES 15 confirms the eastward propagation of the electron cloud.

The magnetic observation of 02 April 2011 event clearly displays the absence of westward electrojet signatures during huge enhancement in the cosmic noise absorption level in the riometer data corresponding to substorm activity. During 10:00–14:00 UT, Maitri is located at the dayside of the magnetosphere. Hence, we would have expected that the precipitation may be due to longitudinal auroral oval expansion up to dayside. Had this been the case, we would have seen the magnitude of auroral electrojet current at Maitri. In an event of strong geomagnetic storm, it is seen that the whole auroral oval is covered with westward electrojet [*Singh et al*., 2015]. However, we do not see any kind of signatures in the *H* component of geomagnetic field at subauroral station, Maitri, during the present event. Hence, this DCNA event is not necessarily due to the ionospheric movement of plasma. Moreover, there is a certain delay of 24 min recorded between the onset of substorm in the *AL* index and onset of CNA in the riometer data that also enhanced electron flux was observed at GOES 13 located at 06:00 MLT. Therefore, absorption event can be attributed to magnetospheric drift of the electrons. The magnetospheric drift of the electrons and protons in the equatorial plane is possible due to the gradient-curvature drift. Figure 9 shows the CNA characteristics at longitudinally distributed stations inside the auroral oval during the substorm on 02 April 2011. Geographic and geomagnetic coordinates of these stations have been given in Table 2. The stations were chosen in such a way that they fall in MLT sector between midnight and Maitri, so that we can examine the electron precipitation at different longitudes during their eastward gradient-curvature drift. Initial selection of the stations for riometer data was chosen from riometer and imaging riometer database given by Department of Physics, Lancaster University, UK (http://spears.lancs.ac.uk/cgi-bin/riometers). The left dashed line shows the onset of the substorm indicated by *AL* index in the first panel. The second to sixth panels from the top show successive delay in the onset time of CNA at longitudinally distributed stations. Please note that stations were plotted eastward from midnight sector to day sector up to Maitri. MCQ being located at magnetic midnight during the onset of the substorm shows immediate onset of CNA, which is mainly due to field line propagation of electron. However, there is a systematic delay in CNA onsets at DAWS, FSIM, RABB, and GILL up to Maitri as we move from west to east. DAWS, FSIM, RABB, and GILL stations are almost equally spaced in MLT. Therefore, we should expect almost same time delay in the CNA onset as we move from one station to another from midnight to Maitri. But, having different *L* values, these stations show little offset from the expected delay time because electron cloud will take slightly more time for larger *L* station as compared to smaller *L* station belonging to the same MLT region. Additionally, the maximum value of CNA has consistently gone down from 3 dB (at MCQ) to 0.8 dB (at Maitri) as one proceeds from midnight to the day sector. This signifies the loss of electrons while drifting eastward. We have taken the delay time between the onset of the substorm

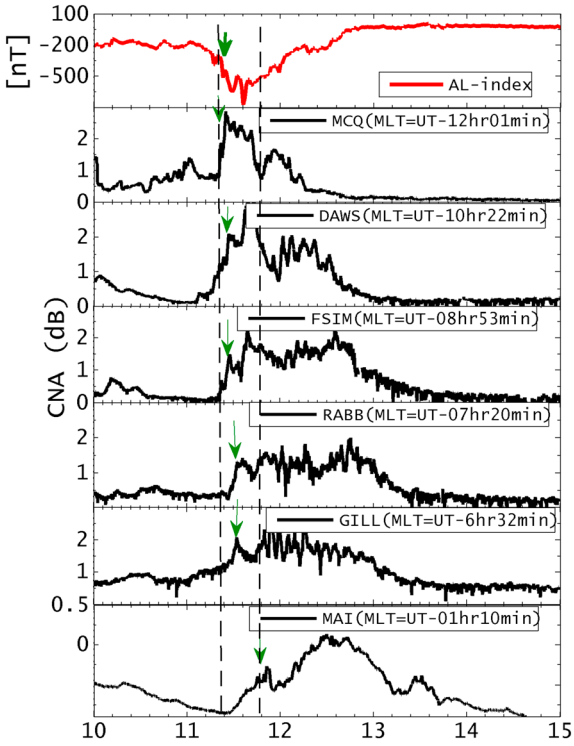

Figure 9. Onsets of CNA at stations in different MLT sectors between local midnight to Maitri location (while approaching eastward) during the substorm onset on 02 April 2011. The green arrow indicates the onset of substorm and CNAs at all the stations. The top plot represents the *AL* index and the rest bottom plots represent the CNA onset at stations mentioned in Table 2.

and onsets of CNA at all the stations to estimate the energy range of the electron flux resulting into CNA at Maitri as well as at other stations.

In degree of magnetic longitude per second ($\frac{Mlong}{time}$), the bounce-averaged drift velocity of electrons in a dipole field can be written as [*Beharrell et al.*, 2015]

$$< w_d >= \frac{3LE}{22\times10^6}(0.7+0.3\sin\alpha_0) \quad (3)$$
$$+4.17\times10^{-3}$$

where L is measured in *Re*, the energy E in eV, and α_0 is the equatorial pitch angle. The value 4.17×10^{-3} is contribution from Earth's rotation [see, e.g., *Northrop*, 1966].

$$t = \frac{\varphi-\varphi'}{< w_d >} + t' \quad (4)$$

Now t is the time taken by an electron to reach at an azimuthal location φ after gradient-curvature drift. For this event, one has to assume the injection of electron after onset at location φ' in t' time [*Beharrell et al.*, 2015]. The above equations clearly show that the drift time is inversely proportional to the energy of the electron flux. If we consider that the CNA is produced due to the energetic electrons that drifted eastward in the equatorial plane due to gradient curvature drift, we have to estimate the energy of the electron flux that actually cause such absorption at $L=5$. To estimate the energy we can rearrange equation (3) and can get the energy equation

$$E = 22\times10^6(0.7+0.3\sin\alpha_0)\left(\frac{1}{3L}\right)[< w_d > -0.00417] \quad (5)$$

$$E = 22\times10^6(0.7+0.3\sin\alpha_0)\left(\frac{1}{3L}\right)\left[\frac{Mlong}{time} - 0.00417\right] \quad (6)$$

Here from equation (6), we can calculate the energy range of electrons that might have caused such precipitation. The upper and lower cutoff of α_0 are, respectively, taken as for the gradient curvature drift in the $L=5$ magnetic shell. Below $\alpha_0=5°$, electrons may fall into loss cone and hence may not take part in the gradient curvature drift. For simplicity we use a single value for equatorial pitch angle, 5° right at the edge of the loss cone where most of the electron flux may likely to get precipitated. To calculate the drift velocity we have used the delay between the substorm onset and the onset of CNA at different stations; e.g., at Maitri, it is ~24 min. Generally, particle injections occur at the magnetic midnight hours during substorm activity [*Liang et al.*, 2007; *Lopez and Lui*, 1990]. Hence, we consider delay as the time of drift of the electrons to reach the location of Maitri. Therefore, the magnetic longitudinal difference of Maitri during the precipitation event will be 153.25°. Hence, after putting all these values in equation (6), the expected energy of the electrons comes 200 keV. Similarly, we calculated the expected energy of the electrons for the other stations. The estimated energy range of electron flux is found to be 170–300 keV. This apparently matches with the enhancement in GOES 13 electron flux observations of energy ranges 150 and 275 keV, which fall within the estimated energy range.

Additionally, pulsation studies of these two events show the presence of Pc5 oscillations on both days. It is clearly seen that the amplitude of Pc5 pulsation is significantly different for both the days. During the dayside

CNA, the peak-to-peak amplitude is ~25 nT, whereas it is <8 nT on the non-CNA event, which is considerably less for this day. This simply explains that the energy transferred into the magnetosphere was higher during the CNA day. Enhanced IEF with increased conductivity during CNA day drives current resulting into increased pulsation amplitude. Hence, we could infer that the energy input to the ionosphere also does play a role in controlling the dayside absorption event. No production of CNA during 14 July 2011 substorm activity is because there is not enough precipitation of keV electrons causing the appreciable absorption in the cosmic noise signal strength as per out criteria mentioned in section 3.1. Lack of enough energetic electron flux together with diminished Pc5 wave power is not favorable condition to scatter significant electron flux causing CNA as to be detected by imaging riometer at Maitri.

6. Conclusions

The current study attempts to examine the detailed characteristics of identified DCNA events observed at Indian Antarctic station Maitri on 02 April 2011. This dayside CNA event is more intense and has larger duration than auroral substorm absorption event that was observed earlier (~05:30 MLT) on the same day at Maitri. Although dayside CNA is related to substorm onsets, the substorm alone is just the necessary condition for the occurrence of such absorption event.

Our comparative study of two substorm events of 02 April 2011 and 14 July 2011 and the detailed examination of DCNA event of 02 April 2011 lead to the following key points:

1. The initial comparison between the characteristics of auroral substorm absorption (ASA) event and the DCNA event at Maitri during 02 April 2011 are distinctively different in characteristics. Absence of westward electrojet and delay between the substorm onset and onset of CNA during the DCNA event indicate different processes involved in ASA and DCNA events. Further, we compare two substorm events when Maitri was in dayside, i.e., one resulting in CNA (02 April 2011) and the other not showing any CNA signature (14 July 2011). The comparison clearly brings out the fact that the substorm can only be the necessary condition to affect the DCNA.
2. Comparison of interplanetary conditions between days of substorms of similar strength when Maitri was in the dayside suggests that longer sustainability (Δt) of higher eastward interplanetary electric field (E_y) favors the DCNA event. However, further statistical study is required to determine if long durations of high IEF E_y are correlated with DCNA occurrence. This will form the part of our future studies.
3. GOES 13 satellite observation of electron fluxes with 40–475 keV energy range shows clear enhancement during substorms on both the days (02 April 2011 and 14 July 2015) when Maitri was on the dayside. However, electron flux in the energy band of 150 and 275 keV during DCNA day have increased by many folds (at least more than twofold) compared to the day of 14 July 2011.
4. Further study of electron cloud evolution for DCNA event (02 April 2011) shows the eastward propagation of these electrons which are encountered by both GOES 13 and GOES 15 satellites (note that GOES 14 was operational in that day but data are not available).
5. For both those days, global presences of Pc5 oscillations were examined. During DCNA, strong Pc5 waves were globally observed. However, for the substorm event not resulting into DCNA, Pc5 wavelike structure was observed for a very short duration both at Maitri and other locations mentioned in Table 2. It should be noted that at Maitri, the peak-to-peak amplitude of this oscillation is 3–4 times larger during DCNA event (11:00–13:00 UT of 02 April 2011) than those observed for no DCNA event (10:00–12:00 UT of 14 July 2011) as depicted in Figure 8. This indicates the presence of pronounced Pc5 oscillations as Maitri facilitates the growth of VLF chorus waves, which in turn trigger the process of loss cone scattering resulting DCNA event through wave-particle interaction as suggested by various researchers working in the area of wave-particle interaction [*Jaynes et al*., 2015, reference therein; *Li et al*., 2011; *Coroniti and Kennel*, 1970].
6. Onsets of CNA at longitudinally distributed stations between the local magnetic midnight and Maitri show systematic time delay. It confirms that the precipitations of eastward drifted electrons are responsible for DCNA event. Further, delays between the substorm onset and onsets of CNA used as the time taken by the eastward drifted electron were used to compute the energy of drifted electrons. It was concluded that electrons in the energy range of 170 to 300 keV might have taken part in the precipitation processes. The inference is in agreement with the observations from GOES 13 and GOES 15 satellites, which also show increment of electron fluxes in the energy band of 150 and 275 keV.

Acknowledgments

We acknowledge the data provision of NORSTAR (University of Alberta, I. Mann) (http://aurora.phys.ucalgary.ca/norstar/index.html); Space Weather Services (SWS), Australia (http://www.sws.bom.gov.au/World_Data_Centre/1/8); INERMAGNET (http://www.intermagnet.org/data-donnee/data-eng.php); OMNI and ACE (NSSDC, N. Papitashvili) (http://omniweb.gsfc.nasa.gov/ow_min.html); and GOES (Space Environment Center, H. Singer) (http://www.ngdc.noaa.gov/stp/satellite/goes/). We also thank JHU/APL for the auroral oval information under OVALATION project (http://sd-www.jhuapl.edu/Aurora/ovation/ovation_display.html). The authors also acknowledge the logistic support provided by National Centre for Antarctic and Ocean Research, Ministry of Earth Sciences, Government of India to conduct studies in Antarctica. They thank the Department of Science and Technology, Government of India for the financial support. We sincerely thank Director, IIG for his support and encouragement.

References

Ansari, Z. A. (1964), The aurorally associated absorption of cosmic noise at college, Alaska, *J. Geophys. Res.*, *69*, 4493–4513, doi:10.1029/JZ069i021p04493.

Arun, T., A. Dhar, K. Emperumal, and B. M. Pathan (2005), IMF B_y dependence of the extent of substorm westward electrojet, *J. Earth Syst. Sci*, *114*, 177–184.

Beharrell, M. J., F. Honary, C. J. Rodger, and M. A. Clilverd (2015), Substorm-induced energetic electron precipitation: Morphology and prediction, *J. Geophys. Res. Space Phys.*, *120*, doi:10.1002/2014JA020632x.

Behera, J. K., A. K. Sinha, A. K. Singh, R. Rawat, G. Vichare, A. Dhar, B. M. Pathan, K. U. Nair, C. Selvaraj, and P. Elango (2014), First results from imaging riometer installed at Indian Antarctic station Maitri, *J. Earth Syst. Sci.*, *123*(3), 593–602.

Behera, J. K., A. K. Sinha, A. K. Singh, G. Vichare, A. Dhar, S. Labde, and K. Jeeva (2015), Substorm related CNA near equatorward boundary of the auroral oval in relation to interplanetary conditions, *Adv. Space Res.*, *56*(1), 28–37, doi:10.1016/j.asr.2015.03.036.

Bortnik, J., and R. M. Thorne (2007), The dual role of ELF/VLF chorus waves in the acceleration and precipitation of radiation belt electrons, *J. Atmos. Sol. Terr. Phys.*, *69*, 377–386.

Codrescu, M. V., T. J. Fuller-Rowell, R. G. Roble, and D. S. Evans (1997), Medium energy particle precipitation influences on the mesosphere and lower thermosphere, *J. Geophys. Res.*, *102*, 19,977–19,987, doi:10.1029/97JA01728.

Coroniti, F., and C. Kennel (1970), Auroral micropulsation instability, *J. Geophys. Res.*, *75*(10), 1863–1878, doi:10.1029/JA075i010p01863.

Detrick, D. L., and T. J. Rosenburg (1990), A phased-array radio wave imager for studies of cosmic noise absorption, *Radio Sci.*, *25*, 325–338, doi:10.1029/RS025i004p00325.

Ding, Y., Z. He, Z. Zhang, and F. Xiao (2013), Influence of wave normal angle on gyroresonance between chorus waves and outer radiation belt electrons, *Sci. China Tech. Sci.*, *56*, 2681–2689, doi:10.1007/s11431-013-5363-6.

Frey, H. U., and S. B. Mende (2006), Substorm onset as observed by IMAGE-FUV, in *Proceedings of the Eighth International Conference on Substorms (ICS-8)*, edited by M. Syrjäsuo and E. Donovan, pp. 71–75 , Univ. of Calgary, Calgary, Alberta, Canada.

Friis-Christensen, E., and J. Wilhjelm (1975), Polar cap currents for different direction of interplanetary magnetic field in the *y-z* plane, *J. Geophys. Res.*, *80*, 1248–1260, doi:10.1029/JA080i010p01248.

Gołkowski, M., and U. S. Inan (2008), Multistation observations of ELF/VLF whistler mode chorus, *J. Geophys. Res.*, *113*, A08210, doi:10.1029/2007JA012977.

Hargreaves, J. K. (2007), Auroral radio absorption: The prediction question, *Adv. Space Res.*, *45*, 1075–1092.

Honary, F., S. R. Marple, K. Barratt, P. Chapman, M. Grill, and E. Nielsen (2011), Digital beam-forming imaging riometer systems, *Rev. Sci. Instrum.*, *82*, 031301, doi:10.1063/1.3567309.

Jaynes, A. N., et al. (2015), Correlated Pc4–5 ULF waves, whistler-mode chorus and pulsating aurora observed by the Van Allen Probes and ground-based systems, *J. Geophys. Res. Space Physics*, *120*, 8749–8761, doi:10.1002/2015JA021380.

Kavanagh, A. J., M. J. Kosch, F. Honary, A. Senior, S. R. Marple, E. E. Woodfield, and I. W. McCrea (2004), The statistical dependence of auroral absorption on geomagnetic and solar wind parameters, *Ann. Geophys.*, *22*, 877–887.

Kavanagh, A. J., F. Honary, E. F. Donovan, T. Ulich, and M. H. Denton (2012), Key features of >30 keV electron precipitation during high speed solar wind streams: A superposed epoch analysis, *J. Geophys. Res.*, *117*, A00L09, doi:10.1029/2011JA017320.

Kleimenova, N. G., O. V. Kozyreva, and H. Ranta (1997), Pc5 pulsations in geomagnetic field and riometer absorption in the down sector of the auroral latitudes (English translation), *Geomagn. Aeron.*, *37*(5), 552–578.

Kleimenova, N. G., O. V. Kozyreva, J. Manninen, and A. Ranta (2005), Unusual strong quasi-monochromatic ground geomagnetic Pc5 pulsations in the recovery phase of November 2003 superstorm, *Ann. Geophys.*, *23*, 2621–2634.

Kremser, G., A. Korth, J. A. Fejer, B. Wilken, A. V. Gurevich, and E. Amata (1981), Observations of quasi-periodic flux variations of energetic ions and electrons associated with Pc5 geomagnetic pulsations, *J. Geophys. Res.*, *86*(A5), 3345–3356, doi:10.1029/JA086iA05p03345.

Li, W., R. M. Thorne, J. Bortnik, Y. Nishimura, and V. Angelopoulos (2011), Modulation of whistler mode chorus waves: 1. Role of compressional Pc4–5 pulsations, *J. Geophys. Res.*, *116*, A06205, doi:10.1029/2010JA016312.

Liang, J., W. W. Liu, E. Spanswick, and E. F. Donovan (2007), Azimuthal structures of substorm electron injection and their signatures in riometer observations, *J. Geophys. Res.*, *112*, A09209, doi:10.1029/2007JA012354.

Little, C. G., and H. Leinbach (1959), The riometer–a device for continuous measurement of ionospheric absorption, *Proc. IRE*, *47*, 315–320.

Lopez, R. E., and A. T. Y. Lui (1990), A multisatellite case study of the expansion of a substorm current wedge in the near-Earth magnetotail, *J. Geophys. Res.*, *95*, 8009–8017, doi:10.1029/JA095iA06p08009.

Manninen, J., N. G. Kleimenova, O. V. Kozyreva, and T. Turunen (2010), Pc5 geomagnetic pulsations, pulsating particle precipitation, and VLF chorus: Case study on 24 November 2006, *J. Geophys. Res.*, *115*, A00F14, doi:10.1029/2009JA014837.

Matthews, D. L., T. J. Rosenberg, J. R. Benbrook, and E. A. Bering III (1988), Dayside energetic electron precipitation over the South Pole (g = 75), *J. Geophys. Res.*, *93*, 12,941–12,945, doi:10.1029/JA093iA11p12941.

Newell, P. T., and C.-I. Meng (1992), Mapping the dayside ionosphere to the magnetosphere according to particle precipitation characteristics, *Geophys. Res. Lett.*, *19*(6), 609–612, doi:10.1029/92GL00404.

Northrop, T. G. (1966), Adiabatic theory of charged particle motion, in *Radiation Trapped in The Earth's Magnetic Field* Proceedings of the Advanced Study Institute Held at the Chr. Michelsen Institute, Bergen, Norway August 16–September 3, 1965, edited by B. M. McCormac, pp. 26–44 , D. Reidel, Dordrecht, Netherlands.

Nosé, M., T. Iyemori, M. Sugiura, A. Slavin, R. A. Hoffman, J. D. Winningham, and N. Sato (1998), Electron precipitation accompanying Pc5 pulsations observed by DE satellites and at a ground station, *J. Geophys. Res.*, *103*(8), 17,587–17,604, doi:10.1029/98JA01187.

Nose, M., et al. (2012), A new substorm index derived from high-resolution geomagnetic field data at low latitude, *Space Weather*, *10*, S08002, doi:10.1029/2012SW000785.

Nyland, I. (2007), A comparison study between cosmic noise absorption and flux of precipitating energetic electrons MSc thesis, Univ. of Bergen, Bergen, Norway.

Øieroset, M., P. E. Sandholt, W. F. Denig, and S. W. H. Cowley (1997), Northward interplanetary magnetic field cusp aurora and high-latitude magnetopause reconnection, *J. Geophys. Res.*, *102*, 11,349–11,362, doi:10.1029/97JA00559.

Østgaard, N., J. Stadsnes, J. Bjordal, R. R. Vondrak, S. A. Cummer, D. Chenette, G. K. Parks, M. J. Brittnacher, and D. L. McKenzie (1999), Global scale electron precipitation features seen in UV and X rays during substorms, *J. Geophys. Res.*, *104*, 10,191–10,204, doi:10.1029/1999JA900004.

Pasmanik, D. L., and V. J. Trakhtengerts (1999), Spectral characteristics of waves and particles in the model of cyclotron wave-particle interactions near plasmapause, *Ann. Geophys.*, *17*(3), 351–357.

Ranta, H., A. Ranta, and J. K. Hargreaves (1999), Small-scale structure of ionospheric absorption of cosmic noise during pre-onset and sharp onset phases of an auroral absorption substorm, *Geophysica*, *35*, 45–57.

Rodger, A. S., S. W. H. Cowley, M. J. Brown, M. Pinnock, and D. A. Simmons (1984), Dawn-dusk (*y*) component of the interplanetary magnetic field and local time of the Harang discontinuity, *Planet. Space Sci.*, *32*, 1021–1027.

Sandholt, P. E., and P. T. Newell (1996), Ground and satellite observations of an auroral event at the cusp/cleft equatorward boundary, *J. Geophys. Res.*, *97*, 8685–8691, doi:10.1029/91JA02995.

Sandholt, P. E., C. J. Farrugia, M. Øieroset, P. Stauning, and S. W. H. Cowley (1996), Auroral signature of lobe reconnection, *Geophys. Res. Lett.*, *23*, 1725–1728, doi:10.1029/96GL01846.

Sandholt, P. E., et al. (2000), Dynamic cusp aurora and associated pulsed reverse convection during northward interplanetary magnetic field, *J. Geophys. Res.*, *105*, 12,869–12,894, doi:10.1029/2000JA900025.

Semeter, J., D. Lummerzheim, and G. Haerendel (2001), Simultaneous multispectral imaging of the discrete aurora, *J. Atmos. Sol. Terr. Phys.*, *63*, 1981–1992.

Singh, A. K., A. K. Sinha, R. Rawat, B. Jayashree, B. M. Pathan, and A. Dhar (2012), A broad climatology of very high latitude substorms, *Adv. Space Res.*, *50*(11), 1512–1523.

Singh, A. K., A. K. Sinha, S. Saini, and R. Rawat (2015), Auroral electrojets during severely disturbed geomagnetic condition on 24 August 2005, *Adv. Space Res.*, *55*(5), 1349–1355, doi:10.1016/j.asr.2014.11.034.

Sinha, A. K., T. K. Yeoman, J. A. Wild, D. M. Wright, S. W. H. Cowley, and A. Balogh (2005), Evidence of transverse magnetospheric field line oscillations as observed from Cluster and ground magnetometers, *Ann. Geophys.*, *23*, 919–929.

Spanswick, E., E. Donovan, and G. Baker (2005), Pc5 modulation of high energy electron precipitation: Particle interaction regions and scattering efficiency, *Ann. Geophys.*, *23*, 1533–1542.

Spanswick, E., E. Donovan, R. Friedel, and A. Korth (2007), Ground based identification of dispersionless electron injections, *Geophys. Res. Lett.*, *34*, L03101, doi:10.1029/2006GL028329.

Stauning, P. (1996), Investigations of ionospheric radio wave absorption processes using imaging riometer techniques, *J. Atmos. Terr. Phys.*, *58*, 753–764.

Su, Z., et al. (2014), Nonstorm time dynamics of electron radiation belts observed by the Van Allen Probes, *Geophys. Res. Lett.*, *41*, 229–235, doi:10.1002/2013GL058912.

Thomas, N., G. Vichare, A. K. Sinha, and R. Rawat (2015), Low-latitude Pi2 oscillations observed by polar Low Earth Orbiting satellite, *J. Geophys. Res. Space Physics*, *120*, 7838–7856, doi:10.1002/2014JA020958.

Xiao, F., Z. Su, H. Zheng, and S. Wang (2009), Modeling of outer radiation belt electrons by multidimensional diffusion process, *J. Geophys. Res.*, *114*, A03201, doi:10.1029/2008JA013580.

Xiao, F., Z. Su, H. Zheng, and S. Wang (2010), Three-dimensional simulations of outer radiation belt electron dynamics including cross diffusion terms, *J. Geophys. Res.*, *115*, A05216, doi:10.1029/2009JA014541.

Xiao, F., et al. (2014), Chorus acceleration of radiation belt relativistic electrons during March 2013 geomagnetic storm, *J. Geophys. Res. Space Physics*, *119*, 3325–3332, doi:10.1002/2014JA019822.